The Astrophysical Journal Supplement Series, 203:28 (14pp), 2012 December doi:10.1088/0067-0049/203/2/28

SWIFT FOLLOW-UP OBSERVATIONS OF CANDIDATE GRAVITATIONAL-WAVE TRANSIENT EVENTS

P. A. Evans[1], J. K. Fridriksson[2], N. Gehrels[3], J. Homan[2], J. P. Osborne[1], M. Siegel[4], A. Beardmore[1], P. Handbauer[5], J. Gelbord[4], J. A. Kennea[4], M. Smith[4], Q. Zhu[4], and The LIGO Scientific Collaboration and Virgo Collaboration, J. Aasi[6], J. Abadie[6], B. P. Abbott[6], R. Abbott[6], T. D. Abbott[7], M. Abernathy[8], T. Accadia[9], F. Acernese[10,11], C. Adams[12], T. Adams[13], P. Addesso[14], R. Adhikari[6], C. Affeldt[15,16], M. Agathos[17], K. Agatsuma[18], P. Ajith[6], B. Allen[15,16,19], A. Allocca[20,21], E. Amador Ceron[19], D. Amariutei[22], S. B. Anderson[6], W. G. Anderson[19], K. Arai[6], M. C. Araya[6], S. Ast[15,16], S. M. Aston[12], P. Astone[23], D. Atkinson[24], P. Aufmuth[15,16], C. Aulbert[15,16], B. E. Aylott[25], S. Babak[26], P. Baker[27], G. Ballardin[28], S. Ballmer[29], Y. Bao[22], J. C. B. Barayoga[6], D. Barker[24], F. Barone[10,11], B. Barr[8], L. Barsotti[30], M. Barsuglia[31], M. A. Barton[24], I. Bartos[32], R. Bassiri[8,33], M. Bastarrika[8], A. Basti[20,34], J. Batch[24], J. Bauchrowitz[15,16], Th. S. Bauer[17], M. Bebronne[9], D. Beck[33], B. Behnke[26], M. Bejger[35], M. G. Beker[17], A. S. Bell[8], C. Bell[8], I. Belopolski[32], M. Benacquista[36], J. M. Berliner[24], A. Bertolini[15,16], J. Betzwieser[12], N. Beveridge[8], P. T. Beyersdorf[37], T. Bhadbade[33], I. A. Bilenko[38], G. Billingsley[6], J. Birch[12], R. Biswas[36], M. Bitossi[20], M. A. Bizouard[39], E. Black[6], J. K. Blackburn[6], L. Blackburn[3], D. Blair[40], B. Bland[24], M. Blom[17], O. Bock[15,16], T. P. Bodiya[30], C. Bogan[15,16], C. Bond[25], R. Bondarescu[4], F. Bondu[41], L. Bonelli[20,34], R. Bonnand[42], R. Bork[6], M. Born[15,16], V. Boschi[20], S. Bose[43], L. Bosi[44], B. Bouhou[31], S. Braccini[20], C. Bradaschia[20], P. R. Brady[19], V. B. Braginsky[38], M. Branchesi[45,46], J. E. Brau[47], J. Breyer[15,16], T. Briant[48], D. O. Bridges[12], A. Brillet[49], M. Brinkmann[15,16], V. Brisson[39], M. Britzger[15,16], A. F. Brooks[6], D. A. Brown[29], T. Bulik[50], H. J. Bulten[17,51], A. Buonanno[52], J. Burguet–Castell[53], D. Buskulic[9], C. Buy[31], R. L. Byer[33], L. Cadonati[54], G. Cagnoli[36,42], E. Calloni[10,55], J. B. Camp[3], P. Campsie[8], K. Cannon[56], B. Canuel[28], J. Cao[57], C. D. Capano[52], F. Carbognani[28], L. Carbone[25], S. Caride[58], S. Caudill[59], M. Cavaglià[60], F. Cavalier[39], R. Cavalieri[28], G. Cella[20], C. Cepeda[6], E. Cesarini[46], T. Chalermsongsak[6], P. Charlton[61], E. Chassande-Mottin[31], W. Chen[57], X. Chen[40], Y. Chen[62], A. Chincarini[63], A. Chiummo[28], H. S. Cho[64], J. Chow[65], N. Christensen[66], S. S. Y. Chua[65], C. T. Y. Chung[67], S. Chung[40], G. Ciani[22], F. Clara[24], D. E. Clark[33], J. A. Clark[54], J. H. Clayton[19], F. Cleva[49], E. Coccia[68,69], P.-F. Cohadon[48], C. N. Colacino[20,34], A. Colla[23,70], M. Colombini[70], A. Conte[23,70], R. Conte[14], D. Cook[24], T. R. Corbitt[30], M. Cordier[37], N. Cornish[27], A. Corsi[6], C. A. Costa[59,71], M. Coughlin[66], J.-P. Coulon[49], P. Couvares[29], D. M. Coward[40], M. Cowart[12], D. C. Coyne[6], J. D. E. Creighton[19], T. D. Creighton[36], A. M. Cruise[25], A. Cumming[8], L. Cunningham[8], E. Cuoco[28], R. M. Cutler[25], K. Dahl[15,16], M. Damjanic[15,16], S. L. Danilishin[40], S. D'Antonio[68], K. Danzmann[15,16], V. Dattilo[28], B. Daudert[6], H. Daveloza[36], M. Davier[39], E. J. Daw[72], R. Day[28], T. Dayanga[43], R. De Rosa[10,55], D. DeBra[33], G. Debreczeni[73], J. Degallaix[42], W. Del Pozzo[17], T. Dent[13], V. Dergachev[6], R. DeRosa[59], S. Dhurandhar[74], L. Di Fiore[10], A. Di Lieto[20,34], I. Di Palma[15,16], M. Di Paolo Emilio[68,75], A. Di Virgilio[20], M. Díaz[36], A. Dietz[9,60], F. Donovan[30], K. L. Dooley[15,16], S. Doravari[6], S. Dorsher[76], M. Drago[77,78], R. W. P. Drever[79], J. C. Driggers[6], Z. Du[57], J.-C. Dumas[40], S. Dwyer[30], T. Eberle[15,16], M. Edgar[8], M. Edwards[13], A. Effler[59], P. Ehrens[6], S. Eikenberry[22], G. Endrőczi[73], R. Engel[6], T. Etzel[6], K. Evans[8], M. Evans[30], T. Evans[12], M. Factourovich[32], V. Fafone[68,69], S. Fairhurst[13], B. F. Farr[80], M. Favata[19], D. Fazi[80], H. Fehrmann[15,16], D. Feldbaum[22], I. Ferrante[20,34], F. Ferrini[28], F. Fidecaro[20,34], L. S. Finn[4], I. Fiori[28], R. P. Fisher[29], R. Flaminio[42], S. Foley[30], E. Forsi[12], L. A. Forte[10], N. Fotopoulos[6], J.-D. Fournier[49], J. Franc[42], S. Franco[39], S. Frasca[23,70], F. Frasconi[20], M. Frede[15,16], M. A. Frei[81], Z. Frei[5], A. Freise[25], R. Frey[47], T. T. Fricke[15,16], D. Friedrich[15,16], P. Fritschel[30], V. V. Frolov[12], M.-K. Fujimoto[18], P. J. Fulda[25], M. Fyffe[12], J. Gair[82], M. Galimberti[42], L. Gammaitoni[44,83], J. Garcia[24], F. Garufi[10,55], M. E. Gáspár[73], G. Gelencser[5], G. Gemme[63], E. Genin[28], A. Gennai[20], L. Á. Gergely[84], S. Ghosh[43], J. A. Giaime[12,59], S. Giampanis[19], K. D. Giardina[12], A. Giazotto[20], S. Gil-Casanova[53], C. Gill[8], J. Gleason[22], E. Goetz[15,16], G. González[59], M. L. Gorodetsky[38], S. Goßler[15,16], R. Gouaty[9], C. Graef[15,16], P. B. Graff[82], M. Granata[42], A. Grant[8], C. Gray[24], R. J. S. Greenhalgh[85], A. M. Gretarsson[86], C. Griffo[7], H. Grote[15,16], K. Grover[25], S. Grunewald[26], G. M. Guidi[45,46], C. Guido[12], R. Gupta[74], E. K. Gustafson[6], R. Gustafson[58], J. M. Hallam[25], D. Hammer[19], G. Hammond[8], J. Hanks[24], C. Hanna[6,87], J. Hanson[12], J. Harms[79], G. M. Harry[88], I. W. Harry[29], E. D. Harstad[47], M. T. Hartman[22], K. Haughian[8], K. Hayama[18], J.-F. Hayau[41], J. Heefner[6], A. Heidmann[48], M. C. Heintze[12], H. Heitmann[49], P. Hello[39], G. Hemming[28], M. A. Hendry[8], I. S. Heng[8], A. W. Heptonstall[6], V. Herrera[33], M. Heurs[15,16], M. Hewitson[15,16], S. Hild[8], D. Hoak[54], K. A. Hodge[6], K. Holt[12], M. Holtrop[89], T. Hong[62], S. Hooper[40], J. Hough[8], E. J. Howell[40], B. Hughey[19], S. Husa[53], S. H. Huttner[8], T. Huynh-Dinh[12], D. R. Ingram[24], R. Inta[65], T. Isogai[66], A. Ivanov[6], K. Izumi[18], M. Jacobson[6], E. James[6], Y. J. Jang[80], P. Jaranowski[90], E. Jesse[86], W. W. Johnson[59], D. I. Jones[91], R. Jones[8], R. J. G. Jonker[17], L. Ju[40], P. Kalmus[6], V. Kalogera[80], S. Kandhasamy[76], G. Kang[92], J. B. Kanner[3,52], M. Kasprzack[28,39], R. Kasturi[93], E. Katsavounidis[30], W. Katzman[12], H. Kaufer[15,16], K. Kaufman[62], K. Kawabe[24], S. Kawamura[18], F. Kawazoe[15,16], D. Keitel[15,16], D. Kelley[29], W. Kells[6], D. G. Keppel[6], Z. Keresztes[84], A. Khalaidovski[15,16], F. Y. Khalili[38], E. A. Khazanov[94], B. K. Kim[92], C. Kim[95], H. Kim[15,16], K. Kim[96], N. Kim[33], Y. M. Kim[64], P. J. King[6], D. L. Kinzel[12], J. S. Kissel[30], S. Klimenko[22], J. Kline[19], K. Kokeyama[59], V. Kondrashov[6], S. Koranda[19], W. Z. Korth[6], I. Kowalska[50], D. Kozak[6], V. Kringel[15,16], B. Krishnan[26], A. Królak[97,98], G. Kuehn[15,16], P. Kumar[29], R. Kumar[8], R. Kurdyumov[33], P. Kwee[30], P. K. Lam[65], M. Landry[24], A. Langley[79], B. Lantz[33],

N. Lastzka[15,16], C. Lawrie[8], A. Lazzarini[6], A. Le Roux[12], P. Leaci[26], C. H. Lee[64], H. K. Lee[96], H. M. Lee[99], J. R. Leong[15,16], I. Leonor[47], N. Leroy[39], N. Letendre[9], V. Lhuillier[24], J. Li[57], T. G. F. Li[17], P. E. Lindquist[6], V. Litvine[6], Y. Liu[57], Z. Liu[22], N. A. Lockerbie[100], D. Lodhia[25], J. Logue[8], M. Lorenzini[45], V. Loriette[101], M. Lormand[12], G. Losurdo[45], J. Lough[29], M. Lubinski[24], H. Lück[15,16], A. P. Lundgren[15,16], J. Macarthur[8], E. Macdonald[8], B. Machenschalk[15,16], M. MacInnis[30], D. M. Macleod[13], M. Mageswaran[6], K. Mailand[6], E. Majorana[23], I. Maksimovic[101], V. Malvezzi[68], N. Man[49], I. Mandel[25], V. Mandic[76], M. Mantovani[20], F. Marchesoni[44,102], F. Marion[9], S. Márka[32], Z. Márka[32], A. Markosyan[33], E. Maros[6], J. Marque[28], F. Martelli[45,46], I. W. Martin[8], R. M. Martin[22], J. N. Marx[6], K. Mason[30], A. Masserot[9], F. Matichard[30], L. Matone[32], R. A. Matzner[103], N. Mavalvala[30], G. Mazzolo[15,16], R. McCarthy[24], D. E. McClelland[65], P. McDaniel[30], S. C. McGuire[104], G. McIntyre[6], J. McIver[54], G. D. Meadors[58], M. Mehmet[15,16], T. Meier[15,16], A. Melatos[67], A. C. Melissinos[105], G. Mendell[24], D. F. Menéndez[4], R. A. Mercer[19], S. Meshkov[6], C. Messenger[13], M. S. Meyer[12], H. Miao[62], C. Michel[42], L. Milano[10,55], J. Miller[65], Y. Minenkov[68], C. M. F. Mingarelli[25], V. P. Mitrofanov[38], G. Mitselmakher[22], R. Mittleman[30], B. Moe[19], M. Mohan[28], S. R. P. Mohapatra[54], D. Moraru[24], G. Moreno[24], N. Morgado[42], A. Morgia[68,69], T. Mori[18], S. R. Morriss[36], S. Mosca[10,55], K. Mossavi[15,16], B. Mours[9], C. M. Mow–Lowry[65], C. L. Mueller[22], G. Mueller[22], S. Mukherjee[36], A. Mullavey[59,65], H. Müller-Ebhardt[15,16], J. Munch[106], D. Murphy[32], P. G. Murray[8], A. Mytidis[22], T. Nash[6], L. Naticchioni[23,70], V. Necula[22], J. Nelson[8], I. Neri[44,83], G. Newton[8], T. Nguyen[65], A. Nishizawa[18], A. Nitz[29], F. Nocera[28], D. Nolting[12], M. E. Normandin[36], L. Nuttall[13], E. Ochsner[19], J. O'Dell[85], E. Oelker[30], G. H. Ogin[6], J. J. Oh[107], S. H. Oh[107], R. G. Oldenberg[19], B. O'Reilly[12], R. O'Shaughnessy[19], C. Osthelder[6], C. D. Ott[62], D. J. Ottaway[106], R. S. Ottens[22], H. Overmier[12], B. J. Owen[4], A. Page[25], L. Palladino[68,75], C. Palomba[23], Y. Pan[52], C. Pankow[19], F. Paoletti[20,28], R. Paoletti[20,21], M. A. Papa[19,26], M. Parisi[10,55], A. Pasqualetti[28], R. Passaquieti[20,34], D. Passuello[20], M. Pedraza[6], S. Penn[93], A. Perreca[29], G. Persichetti[10,55], M. Phelps[6], M. Pichot[49], M. Pickenpack[15,16], F. Piergiovanni[45,46], V. Pierro[108], M. Pihlaja[76], L. Pinard[42], I. M. Pinto[108], M. Pitkin[8], H. J. Pletsch[15,16], M. V. Plissi[8], R. Poggiani[20,34], J. Pöld[15,16], F. Postiglione[14], C. Poux[6], M. Prato[63], V. Predoi[13], T. Prestegard[76], L. R. Price[6], M. Prijatelj[15,16], M. Principe[108], S. Privitera[6], R. Prix[15,16], G. A. Prodi[77,78], L. G. Prokhorov[38], O. Puncken[15,16], M. Punturo[44], P. Puppo[23], V. Quetschke[36], R. Quitzow-James[47], F. J. Raab[24], D. S. Rabeling[17,51], I. Rácz[73], H. Radkins[24], P. Raffai[5,32], M. Rakhmanov[36], C. Ramet[12], B. Rankins[60], P. Rapagnani[23,70], V. Raymond[80], V. Re[68,69], C. M. Reed[24], T. Reed[109], T. Regimbau[49], S. Reid[8], D. H. Reitze[6], F. Ricci[23,70], R. Riesen[12], K. Riles[58], M. Roberts[33], N. A. Robertson[6,8], F. Robinet[39], C. Robinson[13], E. L. Robinson[26], A. Rocchi[68], S. Roddy[12], C. Rodriguez[80], M. Rodruck[24], L. Rolland[9], J. G. Rollins[6], J. D. Romano[36], R. Romano[10,11], J. H. Romie[12], D. Rosińska[35,110], C. Röver[15,16], S. Rowan[8], A. Rüdiger[15,16], P. Ruggi[28], K. Ryan[24], F. Salemi[15,16], L. Sammut[67], V. Sandberg[24], S. Sankar[30], V. Sannibale[6], L. Santamaría[6], I. Santiago-Prieto[8], G. Santostasi[111], E. Saracco[42], B. Sassolas[42], B. S. Sathyaprakash[13], P. R. Saulson[29], R. L. Savage[24], R. Schilling[15,16], R. Schnabel[15,16], R. M. S. Schofield[47], B. Schulz[15,16], B. F. Schutz[13,26], P. Schwinberg[24], J. Scott[8], S. M. Scott[65], F. Seifert[6], D. Sellers[12], D. Sentenac[28], A. Sergeev[94], D. A. Shaddock[65], M. Shaltev[15,16], B. Shapiro[30], P. Shawhan[52], D. H. Shoemaker[30], T. L Sidery[25], X. Siemens[19], D. Sigg[24], D. Simakov[15,16], A. Singer[6], L. Singer[6], A. M. Sintes[53], G. R. Skelton[19], B. J. J. Slagmolen[65], J. Slutsky[59], J. R. Smith[7], M. R. Smith[6], R. J. E. Smith[25], N. D. Smith-Lefebvre[30], K. Somiya[62], B. Sorazu[8], F. C. Speirits[8], L. Sperandio[68,69], M. Stefszky[65], E. Steinert[24], J. Steinlechner[15,16], S. Steinlechner[15,16], S. Steplewski[43], A. Stochino[6], R. Stone[36], K. A. Strain[8], S. E. Strigin[38], A. S. Stroeer[36], R. Sturani[45,46], A. L. Stuver[12], T. Z. Summerscales[112], M. Sung[59], S. Susmithan[40], P. J. Sutton[13], B. Swinkels[28], G. Szeifert[5], M. Tacca[28], L. Taffarello[113], D. Talukder[43], D. B. Tanner[22], S. P. Tarabrin[15,16], R. Taylor[6], A. P. M. ter Braack[17], P. Thomas[24], K. A. Thorne[12], K. S. Thorne[62], E. Thrane[76], A. Thüring[15,16], C. Titsler[4], K. V. Tokmakov[100], C. Tomlinson[72], A. Toncelli[20,34], M. Tonelli[20,34], O. Torre[20,21], C. V. Torres[36], C. I. Torrie[6,8], E. Tournefier[9], F. Travasso[44,83], G. Traylor[12], M. Tse[32], D. Ugolini[114], H. Vahlbruch[15,16], G. Vajente[20,34], J. F. J. van den Brand[17,51], C. Van Den Broeck[17], S. van der Putten[17], A. A. van Veggel[8], S. Vass[6], M. Vasuth[73], R. Vaulin[30], M. Vavoulidis[39], A. Vecchio[25], G. Vedovato[113], J. Veitch[13], P. J. Veitch[106], K. Venkateswara[115], D. Verkindt[9], F. Vetrano[45,46], A. Viceré[45,46], A. E. Villar[6], J.-Y. Vinet[49], S. Vitale[17], H. Vocca[44], C. Vorvick[24], S. P. Vyatchanin[38], A. Wade[65], L. Wade[19], M. Wade[19], S. J. Waldman[30], L. Wallace[6], Y. Wan[57], M. Wang[25], X. Wang[57], A. Wanner[15,16], R. L. Ward[31], M. Was[39], M. Weinert[15,16], A. J. Weinstein[6], R. Weiss[30], T. Welborn[12], L. Wen[40,62], P. Wessels[15,16], M. West[29], T. Westphal[15,16], K. Wette[15,16], J. T. Whelan[81], S. E. Whitcomb[6,40], D. J. White[72], B. F. Whiting[22], K. Wiesner[15,16], C. Wilkinson[24], P. A. Willems[6], L. Williams[22], R. Williams[6], B. Willke[15,16], M. Wimmer[15,16], L. Winkelmann[15,16], W. Winkler[15,16], C. C. Wipf[30], A. G. Wiseman[19], H. Wittel[15,16], G. Woan[8], R. Wooley[12], J. Worden[24], J. Yablon[80], I. Yakushin[12], H. Yamamoto[6], K. Yamamoto[78,116], C. C. Yancey[52], H. Yang[62], D. Yeaton-Massey[6], S. Yoshida[117], M. Yvert[9], A. Zadrożny[98], M. Zanolin[86], J.-P. Zendri[113], F. Zhang[57], L. Zhang[6], C. Zhao[40], N. Zotov[109], M. E. Zucker[30], and J. Zweizig[6]

[1] Department of Physics and Astronomy, University of Leicester, Leicester, LE1 7RH, UK
[2] MIT Kavli Institute for Astrophysics and Space Research, 77 Massachusetts Avenue, Cambridge, MA 02139, USA
[3] NASA Goddard Space Flight Center, Greenbelt, MD 20771, USA
[4] The Pennsylvania State University, University Park, PA 16802, USA
[5] Eötvös Loránd University, Budapest, 1117 Hungary
[6] LIGO-California Institute of Technology, Pasadena, CA 91125, USA

[7] California State University Fullerton, Fullerton, CA 92831, USA
[8] SUPA, University of Glasgow, Glasgow, G12 8QQ, UK
[9] Laboratoire d'Annecy-le-Vieux de Physique des Particules (LAPP), Université de Savoie, CNRS/IN2P3, F-74941 Annecy-Le-Vieux, France
[10] INFN, Sezione di Napoli, Complesso Universitario di Monte S. Angelo, I-80126 Napoli, Italy
[11] Università di Salerno, Fisciano, I-84084 Salerno, Italy
[12] LIGO-Livingston Observatory, Livingston, LA 70754, USA
[13] Cardiff University, Cardiff, CF24 3AA, UK
[14] University of Salerno, I-84084 Fisciano (Salerno), Italy
[15] Albert-Einstein-Institut, Max-Planck-Institut für Gravitationsphysik, D-30167 Hannover, Germany
[16] Leibniz Universität Hannover, D-30167 Hannover, Germany
[17] Nikhef, Science Park, Amsterdam, The Netherlands
[18] National Astronomical Observatory of Japan, Tokyo 181-8588, Japan
[19] University of Wisconsin–Milwaukee, Milwaukee, WI 53201, USA
[20] INFN, Sezione di Pisa, I-56127 Pisa, Italy
[21] Università di Siena, I-53100 Siena, Italy
[22] University of Florida, Gainesville, FL 32611, USA
[23] INFN, Sezione di Roma, I-00185 Roma, Italy
[24] LIGO-Hanford Observatory, Richland, WA 99352, USA
[25] University of Birmingham, Birmingham, B15 2TT, UK
[26] Albert-Einstein-Institut, Max-Planck-Institut für Gravitationsphysik, D-14476 Golm, Germany
[27] Montana State University, Bozeman, MT 59717, USA
[28] European Gravitational Observatory (EGO), I-56021 Cascina (PI), Italy
[29] Syracuse University, Syracuse, NY 13244, USA
[30] LIGO-Massachusetts Institute of Technology, Cambridge, MA 02139, USA
[31] APC, AstroParticule et Cosmologie, Université Paris Diderot, CNRS/IN2P3, CEA/Irfu, Observatoire de Paris, Sorbonne Paris Cité, 10, rue Alice Domon et Léonie Duquet, F-75205 Paris Cedex 13, France
[32] Columbia University, New York, NY 10027, USA
[33] Stanford University, Stanford, CA 94305, USA
[34] Università di Pisa, I-56127 Pisa, Italy
[35] CAMK-PAN 00-716 Warsaw, Poland
[36] The University of Texas at Brownsville, Brownsville, TX 78520, USA
[37] San Jose State University, San Jose, CA 95192, USA
[38] Moscow State University, Moscow, 119992, Russia
[39] LAL, Université Paris-Sud, IN2P3/CNRS, F-91898 Orsay, France
[40] University of Western Australia, Crawley, WA 6009, Australia
[41] Institut de Physique de Rennes, CNRS, Université de Rennes 1, F-35042 Rennes, France
[42] Laboratoire des Matériaux Avancés (LMA), IN2P3/CNRS, F-69622 Villeurbanne, Lyon, France
[43] Washington State University, Pullman, WA 99164, USA
[44] INFN, Sezione di Perugia, I-06123 Perugia, Italy
[45] INFN, Sezione di Firenze, I-50019 Sesto Fiorentino, Italy
[46] Università degli Studi di Urbino "Carlo Bo", I-61029 Urbino, Italy
[47] University of Oregon, Eugene, OR 97403, USA
[48] Laboratoire Kastler Brossel, ENS, CNRS, UPMC, Université Pierre et Marie Curie, 4 Place Jussieu, F-75005 Paris, France
[49] Université Nice-Sophia-Antipolis, CNRS, Observatoire de la Côte d'Azur, F-06304 Nice, France
[50] Astronomical Observatory, Warsaw University, 00-478 Warsaw, Poland
[51] VU University Amsterdam, De Boelelaan 1081, 1081 HV Amsterdam, The Netherlands
[52] University of Maryland, College Park, MD 20742, USA
[53] Universitat de les Illes Balears, E-07122 Palma de Mallorca, Spain
[54] University of Massachusetts-Amherst, Amherst, MA 01003, USA
[55] Università di Napoli "Federico II", Complesso Universitario di Monte S. Angelo, I-80126 Napoli, Italy
[56] Canadian Institute for Theoretical Astrophysics, University of Toronto, Toronto, Ontario, M5S 3H8, Canada
[57] Tsinghua University, Beijing 100084, China
[58] University of Michigan, Ann Arbor, MI 48109, USA
[59] Louisiana State University, Baton Rouge, LA 70803, USA
[60] The University of Mississippi, University, MS 38677, USA
[61] Charles Sturt University, Wagga, NSW 2678, Australia
[62] Caltech-CaRT, Pasadena, CA 91125, USA
[63] INFN, Sezione di Genova, I-16146 Genova, Italy
[64] Pusan National University, Busan 609-735, Republic of Korea
[65] Australian National University, Canberra, ACT 0200, Australia
[66] Carleton College, Northfield, MN 55057, USA
[67] The University of Melbourne, Parkville, VIC 3010, Australia
[68] INFN, Sezione di Roma Tor Vergata, Italy
[69] Università di Roma Tor Vergata, I-00133 Roma, Italy
[70] Università "La Sapienza", I-00185 Roma, Italy
[71] Instituto Nacional de Pesquisas Espaciais, 12227-010 - São José dos Campos, SP, Brazil
[72] The University of Sheffield, Sheffield S10 2TN, UK
[73] Wigner RCP, RMKI, H-1121 Budapest, Konkoly Thege Miklós út 29-33, Hungary
[74] Inter-University Centre for Astronomy and Astrophysics, Pune - 411007, India
[75] Università dell'Aquila, I-67100 L'Aquila, Italy
[76] University of Minnesota, Minneapolis, MN 55455, USA
[77] INFN, Gruppo Collegato di Trento, I-38050 Povo, Trento, Italy
[78] Università di Trento, I-38050 Povo, Trento, Italy
[79] California Institute of Technology, Pasadena, CA 91125, USA
[80] Northwestern University, Evanston, IL 60208, USA
[81] Rochester Institute of Technology, Rochester, NY 14623, USA

[82] University of Cambridge, Cambridge, CB2 1TN, UK
[83] Università di Perugia, I-06123 Perugia, Italy
[84] University of Szeged, 6720 Szeged, Dóm tér 9, Hungary
[85] Rutherford Appleton Laboratory, HSIC, Chilton, Didcot, Oxon OX11 0QX, UK
[86] Embry-Riddle Aeronautical University, Prescott, AZ 86301, USA
[87] Perimeter Institute for Theoretical Physics, Ontario, N2L 2Y5, Canada
[88] American University, Washington, DC 20016, USA
[89] University of New Hampshire, Durham, NH 03824, USA
[90] Białystok University 15-424 Białystok, Poland
[91] University of Southampton, Southampton, SO17 1BJ, UK
[92] Korea Institute of Science and Technology Information, Daejeon 305-806, Republic of Korea
[93] Hobart and William Smith Colleges, Geneva, NY 14456, USA
[94] Institute of Applied Physics, Nizhny Novgorod, 603950, Russia
[95] Lund Observatory, Box 43, SE-221 00, Lund, Sweden
[96] Hanyang University, Seoul 133-791, Republic of Korea
[97] IM-PAN 00-956 Warsaw, Poland
[98] NCBJ 05-400 Świerk-Otwock, Poland
[99] Seoul National University, Seoul 151-742, Republic of Korea
[100] University of Strathclyde, Glasgow, G1 1XQ, UK
[101] ESPCI, CNRS, F-75005 Paris, France
[102] Dipartimento di Fisica, Università di Camerino, I-62032 Camerino, Italy
[103] The University of Texas at Austin, Austin, TX 78712, USA
[104] Southern University and A&M College, Baton Rouge, LA 70813, USA
[105] University of Rochester, Rochester, NY 14627, USA
[106] University of Adelaide, Adelaide, SA 5005, Australia
[107] National Institute for Mathematical Sciences, Daejeon 305-390, Republic of Korea
[108] University of Sannio at Benevento, I-82100 Benevento, Italy and INFN (Sezione di Napoli), Italy
[109] Louisiana Tech University, Ruston, LA 71272, USA
[110] Institute of Astronomy 65-265 Zielona Góra, Poland
[111] McNeese State University, Lake Charles, LA 70609, USA
[112] Andrews University, Berrien Springs, MI 49104, USA
[113] INFN, Sezione di Padova, I-35131 Padova, Italy
[114] Trinity University, San Antonio, TX 78212, USA
[115] University of Washington, Seattle, WA, 98195-4290, USA
[116] Università di Padova, I-35131 Padova, Italy
[117] Southeastern Louisiana University, Hammond, LA 70402, USA
Received 2012 May 25; accepted 2012 October 25; published 2012 November 21

ABSTRACT

We present the first multi-wavelength follow-up observations of two candidate gravitational-wave (GW) transient events recorded by LIGO and Virgo in their 2009–2010 science run. The events were selected with low latency by the network of GW detectors (within less than 10 minutes) and their candidate sky locations were observed by the *Swift* observatory (within 12 hr). Image transient detection was used to analyze the collected electromagnetic data, which were found to be consistent with background. Off-line analysis of the GW data alone has also established that the selected GW events show no evidence of an astrophysical origin; one of them is consistent with background and the other one was a test, part of a "blind injection challenge." With this work we demonstrate the feasibility of rapid follow-ups of GW transients and establish the sensitivity improvement joint electromagnetic and GW observations could bring. This is a first step toward an electromagnetic follow-up program in the regime of routine detections with the advanced GW instruments expected within this decade. In that regime, multi-wavelength observations will play a significant role in completing the astrophysical identification of GW sources. We present the methods and results from this first combined analysis and discuss its implications in terms of sensitivity for the present and future instruments.

Key words: gravitational waves – ultraviolet: general – X-rays: general

1. INTRODUCTION

Some of the key questions in the pursuit of sources of transient gravitational radiation detectable by LIGO (Abbott et al. 2009) and Virgo (Accadia et al. 2012) relate to their electromagnetic (EM) signatures and our ability to observe them (Abadie et al. 2012a). In several of these sources, such as core-collapse supernovae and neutron-star–neutron-star or neutron-star–black-hole mergers, energetics suggest gravitational waves (GWs) are likely to be accompanied by EM emission across the spectrum and over timescales ranging from seconds to days (Fryer et al. 2002; Piran 2004; Mészáros 2006; Nakar 2007; Corsi & Mészáros 2009). Multi-wavelength EM observations of such events have already set the paradigm for improved constraints on source astrophysics set jointly rather than separately. Prompt outbursts, as well as afterglows in X-ray, optical, and radio associated with gamma-ray bursts (GRBs) and supernovae have shed light on the progenitors and the astrophysics of these systems (Kulkarni et al. 1998; Bloom et al. 1999; Matheson et al. 2003; Berger et al. 2005; Gehrels et al. 2005; Soderberg et al. 2005, 2010; Berger 2009, 2011; Zhang & MacFadyen 2009). The benefit of coupling them to GW observations will be tremendous as this will bring the GW observations into astrophysical and cosmological context. Besides increasing detection confidence

(Kochanek & Piran 1993), multi-wavelength observations may improve source localization down to the arcsecond level, leading to identification of the host galaxy and measurement of the redshift (Schutz 1986; Sylvestre 2003; Stubbs 2008; Phinney 2009; Stamatikos et al. 2009; Bloom et al. 2009; Metzger et al. 2010; Metzger & Berger 2012). Conversely, the absence of any EM signature for an otherwise confident transient detection with the GW detectors alone will provide constraints on emission mechanisms, progenitors, and energetics.

LIGO (Abbott et al. 2009) and Virgo (Accadia et al. 2012) form a network of interferometric detectors aiming to make the first direct observations of GWs. In their 2009–2010 data-taking period this network consisted of three interferometers: LIGO-Hanford in Washington State in the USA, LIGO-Livingston in Louisiana in the USA, and Virgo in Italy. During these science runs of the instruments we implemented a first program that could allow prompt EM follow-up of candidate GW transients. Starting with GW data, low-latency searches for compact binary star coalescences (Abadie et al. 2011a) and un-modeled GW transients were performed. This allowed the prompt identification and sky localization of GW candidates, which for the first time were passed on to ground-based telescopes and *Swift* in order to be followed up. In an earlier publication (Abadie et al. 2012a) we presented the details of the implementation and testing of this low-latency search and its coupling to EM astronomy. In this paper we report on the analysis of the *Swift* data we collected as part of this program.

With the start of the 2009–2010 LIGO–Virgo runs we established a Target-of-Opportunity (ToO) program with *Swift* in order to search for possible afterglow in X-ray, ultraviolet, and optical wavelengths of a small number of GW transient candidates. The sensitivity of the GW detectors at the time made the chance of a detection small, but non-negligible. For the case of binary sources with at least one neutron star in the system, the rate of detectable merger events was predicted to be in the range of 2.7×10^{-4} to 0.3 events per year (Abadie et al. 2010a). This ToO program was exercised twice; neither time led to detection of an EM counterpart to a GW transient. Nonetheless, the program addressed implementation questions and established the first joint observation and coordinated data analysis by the LIGO–Virgo network and *Swift* satellite.

In this paper we present the results from the EM follow-up program involving only *Swift*; results from the sister program involving the follow-up of GW candidates by ground-based optical and radio telescopes will be the subject of a forthcoming publication. The paper is organized as follows. In Section 2 we describe the *Swift* observatory. Then, in Section 3, we review the procedure for targeting EM follow-up of GW events, as described in detail in Abadie et al. (2012a). The *Swift* observations and analysis of data are described in Section 4. In Section 5 we present our formalism for combining results from the joint GW–EM search, including the simulation work we performed. We conclude in Section 6 with a discussion and outlook for this kind of joint search.

2. THE *SWIFT* OBSERVATORY

The *Swift* Gamma-Ray Burst Mission (Gehrels et al. 2004), developed and launched under NASA's Medium Explorer Program, is unique for its broad wavelength sensitivity and rapid response. Three telescopes are co-aligned. The Burst Alert Telescope (BAT; Barthelmy et al. 2005) is a broad field of view (FOV) coded-aperture instrument with a CdZnTe detector plane, designed to search for transient events such as GRBs. Approximately 100 GRBs are discovered by BAT each year. In response to a BAT trigger, the spacecraft performs an autonomous slew to point the two narrow FOV instruments. The Ultra-Violet and Optical Telescope (UVOT; Roming et al. 2005) performs follow-up observations of GRBs in the 170–600 nm band, with a $0.^{\circ}28 \times 0.^{\circ}28$ FOV. The X-Ray Telescope (XRT; Burrows et al. 2005) has an effective area peaking at 110 cm^2 (at 1.5 keV), a $0.^{\circ}4 \times 0.^{\circ}4$ FOV, and an energy bandpass of 0.3–10 keV. While spacecraft slewing can be initiated autonomously, achieving repointing within approximately 2 minutes, the process can also be initiated from the ground. The *Swift* Mission Operations Center, located near the University Park campus of the Pennsylvania State University, receives over 1000 requests for ToOs from the astronomical community each year. Response time to a ToO depends on scientific priority and urgency. Due to communication limitations and human-in-the-loop commanding, observation of the highest priority ToOs is typically achieved within 4 hr, although frequently the response time is less than 1 hr. In this way, a ground-based observatory such as LIGO–Virgo can provide the trigger for a transient event, with *Swift* providing prompt follow-up observations in the X-ray, UV, and optical bands.

3. SELECTION OF GRAVITATIONAL-WAVE TRANSIENTS

The LIGO–Virgo EM follow-up program took place during two observing periods spanning a bit over two months from 2009 December 17 to 2010 January 8 and from 2010 September 2 to 2010 October 20. The details of the implementation and testing of the end-to-end search on the GW end have been described elsewhere (Abadie et al. 2012a). Here we will summarize the key features and expand on aspects that were specific to the joint program with *Swift*.

3.1. Event Selection

GW candidate events were selected for follow-up based primarily on their False Alarm Rate (FAR), the rate at which an event of equal or greater significance is expected to occur in the absence of a true signal. For this run, in order to trigger a *Swift* follow-up, we set a nominal threshold on the candidate events' FAR at no more than one event per 35 days of triple coincident running (i.e., the GW instrument configuration when all three detectors were acquiring sensitive data).

To avoid trying to image unusually poorly localized events, an additional constraint was placed on candidates that 20% or more of the a posteriori (see Section 3.2) weighted probability in the event skymap must be covered by up to five $0.^{\circ}4 \times 0.^{\circ}4$ tiles selected for follow-up as *Swift* fields. The number of fields picked for the *Swift* follow-up program reflected a compromise between the need to cover as large an area in the sky as possible and the requirement to be minimally disruptive of *Swift*'s other science targets. If five fields were targeted by *Swift* for each LIGO–Virgo candidate, the correct location of GW events of high significance could be imaged with a probability greater than 50% (Abadie et al. 2012a). Additionally, manual and automated checks were performed on data quality in each interferometer before sending any alerts, eliminating events which had an obvious problem associated with them. For events which passed all data selection criteria, observation requests were sent to *Swift* through web-based ToO submission.[118]

[118] https://www.swift.psu.edu/secure/toop/too_request.htm

During the course of the EM follow-up program, GW candidate transient events were selected by transient-finding algorithms for un-modeled bursts as well as compact binary star coalescences (Abadie et al. 2012a). Two such events met all criteria and were submitted for follow-up with *Swift*. These were identified by one of the generic transient-finding algorithms, called coherent WaveBurst (Klimenko et al. 2011). This algorithm uses wavelet decomposition to search for GWs without relying on specific waveform models. The "January" event occurred at 8:46 UTC on 2010 January 7. This was an event close to the end of the first LIGO–Virgo observation period, during which we lowered the nominal thresholds to 1 event per day for the FAR and 10% for the weighted probability of the event skymap. The thresholds were adjusted as the first LIGO–Virgo observation period was approaching an end in order to exercise the follow-up process at least once. The "September" event, which occurred at 6:42 UTC on 2010 September 16, passed all nominal criteria for follow-ups. This event was later (in 2011 March) revealed to be a "blind injection" artificially inserted into the interferometers as a test of our detection procedures (Abadie et al. 2011b, 2011c, 2012b). While both of these events were ultimately tests of the system rather than plausible candidates, they demonstrate the viability of performing rapid follow-ups of potential GW signals using *Swift*.

3.2. Position Errors and Tiling

The typical uncertainty in sky location of a GW signal is large (typically tens of square degrees) relative to the FOV of *Swift*'s XRT and UVOT instruments. This may be in part addressed by imposing the requirement for the reconstructed sky location to overlap with nearby galaxies. We have used information from the Gravitational Wave Galaxy Catalog (GWGC; White et al. 2011) in order to fold into the tiling algorithm location, extent, and blue luminosity of known galaxies within a distance less than 50 Mpc, since the GW interferometer network would not be likely to detect neutron star binary coalescences beyond this distance. In this way, locations with a known galaxy from this catalog were given greater weight than those without galaxies present.

For the earlier "winter" run in which the January event occurred, skymap tiles with galaxies or globular clusters at a distance less than 50 Mpc had their estimated probability increased by a factor of three, whereas for the later "autumn" run the estimated relative probability of each tile in the skymap was calculated according to

$$P \propto \sum_i \frac{M_i L}{D_i}, \quad (1)$$

where M_i is the blue light luminosity of a galaxy (a proxy for star formation rate; Phinney 1991; Kopparapu et al. 2008; Abadie et al. 2010a), L is the likelihood from only the GW skymap, and D_i is the distance of the galaxy from Earth (Nuttall & Sutton 2010). The index i sums over each galaxy associated with the skymap tile. Only ~8% of tiles in a typical skymap were associated with one or more galaxies, while P was set to zero for tiles with no associated galaxy (Abadie et al. 2012a). After this summation was performed, the resulting likelihoods were renormalized to a probability of unity over the entire skymap. In this way we constructed the a posteriori probability skymaps that we used for prioritizing the *Swift* observations.

For both events selected for follow-up, several tiles were chosen and passed on for imaging as *Swift* fields according to the procedures outlined above. The probability skymaps produced by coherent WaveBurst without galaxy weighting and containing the top 1000 tiles are shown in Figure 1. The maps show large spreads in probability on the sky, the first due to their relatively low significance, the second due to worse sensitivity in Virgo relative to the LIGO interferometers. Simulations show that, despite the relatively small size of *Swift* fields with respect to the extent of our probability skymaps, sources originating in or close to nearby galaxies can be correctly localized with reasonable success rates (see Abadie et al. 2012a and discussion in Section 5). The regions containing the fields imaged by *Swift* are shown with an asterisk on each skymap, with precise coordinates of each field given in Tables 1 and 2.

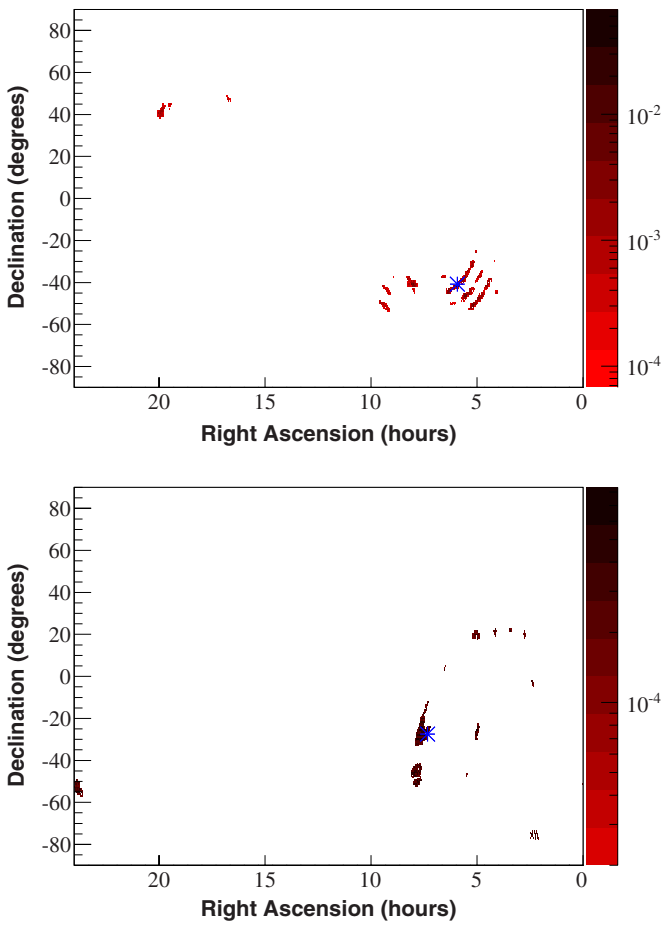

Figure 1. Probability skymaps of the January event (top) and September event (bottom) as determined by the coherent WaveBurst algorithm before galaxy weighting. The asterisks mark the approximate locations of the locations selected for follow-up with *Swift*. Color scale shows fraction of total (raw) probability contained within that particular skymap tile.

4. OBSERVATIONS WITH *SWIFT*

The ToO requests were submitted manually via the Web within 2 hr from the collection of GW data. The initial two requested pointings for each event were submitted as "high priority" (but not the highest); this reflected a compromise between capturing the early light and being minimally disruptive to *Swift* operations. *Swift* observations with the XRT and UVOT instruments of the specified targets were performed in the following ~12 hr. Rapid follow-up could significantly increase the likelihood of a detection, as several types of potential GW/EM sources (e.g., short GRBs) have afterglows that fade

Table 1
Details of the *Swift*-XRT Follow-up Observations of the January Event

Swift ObsID	Date Start (UT)	Date End (UT)	Exposure (ks)	Pointing Direction J2000
00031575001	2010 Jan 7 at 13:04	2011 Jan 7 at 14:29	1.5	89.°07, −40.°96
00031575002	2010 Jan 11 at 19:11	2010 Jan 11 at 19:38	1.6	89.°00, −40.°92
00031576001	2010 Jan 7 at 14:33	2010 Jan 7 at 15:55	1.7	89.°14, −40.°80
00031576002	2010 Jan 11 at 15:59	2010 Jan 11 at 16:18	1.1	89.°13, −40.°77
00031577001	2010 Jan 7 at 15:57	2010 Jan 7 at 17:20	1.8	88.°60, −40.°81
00031577002	2010 Jan 11 at 17:35	2010 Jan 11 at 18:02	1.6	88.°60, −40.°76
00031578001	2010 Jan 7 at 17:23	2010 Jan 7 at 18:49	2.0	88.°07, −40.°79
00031578002	2010 Jan 11 at 13:18	2010 Jan 11 at 15:01	1.4	88.°06, −40.°78
00031579001	2010 Jan 7 at 20:26	2010 Jan 7 at 20:59	2.0	88.°71, −41.°16
00031579002	2010 Jan 11 at 18:03	2010 Jan 11 at 19:51	1.4	88.°77, −41.°17

Table 2
Details of the *Swift*-XRT Follow-up Observations of the September Event

Swift Observation	Date Start (UT)	Date End (UT)	Exposure (ks)	Pointing Direction J2000
00031825001	2010 Sep 16 at 18:10	2010 Sep 16 at 18:35	1.5	110.°98, −27.°53
00031825002	2010 Dec 30 at 03:17	2010 Dec 30 at 03:19	0.09	110.°98, −27.°54
00031825003	2010 Dec 30 at 00:06	2010 Dec 30 at 03:34	2.3	110.°98, −27.°53
00031826001	2010 Sep 16 at 19 36	2010 Sep 16 at 20:09	2.0	109.°86, −27.°57
00031826002	2010 Dec 29 at 03:37	2010 Dec 29 at 04:50	0.14	109.°85, −27.°54
00031826003	2010 Dec 29 at 03:38	2010 Dec 29 at 05:09	1.9	109.°86, −27.°58

below detectability on a timescale of ∼hours. The highest probability region of the January event skymap was observed by *Swift* in five overlapping fields (Figure 2). Each of these was observed twice that month. For the September event two disjoint *Swift* fields were observed (Figure 2). Note that the fields shown are explicitly for the XRT analysis, whereas the UVOT has a slightly smaller FOV. Each September event field was observed on two days, one in 2010 September and the other in 2010 December. Details of the observations are given in Tables 1 and 2.

4.1. X-Ray Results

We analyzed the *Swift*-XRT data with custom scripts which use the software described in Evans et al. (2007, 2009). For each field we combined the observations and produced a single image and exposure map. We then used the source detection and point-spread function (PSF) fitting code described in Goad et al. (2007) and Evans et al. (2009) to identify and localize sources in the field. This method uses a sliding-cell detection algorithm, with a fixed cell size of 21 × 21 pixels (49.″6 × 49.″6, which encloses 93% of the PSF). An initial run with a detection significance threshold of 3 (i.e., S/σ_S is at least 3, where S is the estimated number of net source counts in the cell, and σ_S is the uncertainty in this value, determined using the background estimated from an annular box of size 51 pixels) revealed no sources in any of the observations, however for faint sources this box size is sub-optimal. We performed a second source search with a reduced detection threshold of 1.5σ. We measured the mean background level in each field and, using a circular source region of radius 10 pixels centered on the position of each of these "reduced-threshold" detections, we applied the Bayesian test of Kraft et al. (1991), only accepting sources which this test determined to be detected with at least 99.7% confidence (i.e., 3σ detections). While this method makes us more sensitive to faint sources, it also increases likelihood of getting false positives due to background inhomogeneities, thus these detections should be treated with caution. A detection system optimized for faint sources is under development. The positions of the reduced-threshold detections are given in Tables 3 and 4.

Each of these reduced-threshold detections had very few photons, therefore it was not useful to perform a detailed spectral analysis. We determined the mean count-rate of each detection using the Bayesian method of Kraft et al. (1991) and then applied corrections for PSF losses and instrumental effects, following the processes described by Evans et al. (2007, 2009). We used PIMMS[119] to determine a count-rate-to-flux-conversion factor, assuming an absorbed power-law spectrum with a photon index of 1.7. For the January event the assumed absorbing column was 4×10^{20} cm^{-2}, giving a 0.3–10 keV conversion factor of 4.2×10^{-11} erg cm^{-2} counts^{-1}; for the September event the absorbing column was 3×10^{21} cm^{-2}, giving a 0.3–10 keV conversion factor of 5.1×10^{-11} erg cm^{-2} counts^{-1}. A change of 0.2 in the assumed index of the power-law spectrum would result in a ∼10% change in these conversion factors. The absorbing columns were taken as the Galactic values in the direction of the event, determined from Kalberla et al. (2005) assuming the abundances of Anders & Grevesse (1989).

Given the sky area covered by the *Swift* observations (0.126 square degrees per XRT field after instrumental corrections are applied) we expect to find a number of serendipitous sources in the XRT data. To quantify the likelihood of serendipitous source detection, we used the 2XMMi-DR3 catalogue (Watson et al. 2009), which is substantially dominated by serendipitous X-ray sources found by the *XMM-Newton* observatory (Jansen et al. 2001).

We selected from this catalogue all unique good sources (i.e., with a quality flag of 0; for the flag definition see Watson et al. 2009). For consistency with 2XMMi-DR3 we

[119] http://heasarc.nasa.gov/Tools/w3pimms.html

Table 3
The Reduced-threshold Detections in the X-Ray Data for the January Event

Source	Right Ascension (R.A.) (J2000)	Declination (decl.) (J2000)	Position Error (″ 90% conf.)	Count-rate (0.3–10 keV, ks^{-1})	N_s[a]	Variability[b] Significance (σ)
1	$05^h55^m1\overset{s}{.}00$	$-40°58'00\overset{''}{.}8$	4.5	$5.9^{+1.5}_{-1.2}$	0.9	2.05
2	$05^h57^m4\overset{s}{.}80$	$-40°54'45\overset{''}{.}4$	4.3	$5.9^{+2.1}_{-1.6}$	0.9	0.26
3	$05^h54^m12\overset{s}{.}72$	$-40°44'05\overset{''}{.}8$	4.3	$4.6^{+1.5}_{-1.2}$	1.3	0.45
4	$05^h54^m59\overset{s}{.}29$	$-40°54'19\overset{''}{.}6$	4.5	$3.2^{+1.3}_{-1.0}$	2.4	0.75
5	$05^h51^m57\overset{s}{.}66$	$-40°46'10\overset{''}{.}9$	5.6	$2.8^{+1.8}_{-1.1}$	2.9	1.10
6	$05^h51^m41\overset{s}{.}12$	$-40°44'46\overset{''}{.}4$	5.5	$1.4^{+1.1}_{-0.7}$	7.5	0.74
7	$05^h52^m6\overset{s}{.}29$	$-40°59'14\overset{''}{.}3$	6.5	$2.3^{+1.2}_{-0.8}$	3.9	0.91
8	$05^h52^m55\overset{s}{.}88$	$-40°46'14\overset{''}{.}9$	5.2	$2.9^{+1.7}_{-1.2}$	2.8	2.00

Notes.
[a] N_s is the number of 2XMMi-DR3 sources which are at least as bright as the *Swift* source, which are expected in a single *Swift* field. See the text for details.
[b] The significance of the difference in count-rate between the difference epoch observations.

Table 4
The Reduced-threshold Detections in the X-Ray Data for the September Event

Source	Right Ascension (R.A.) (J2000)	Declination (decl.) (J2000)	Position Error (″ 90% Conf.)	Count-rate (0.3–10 keV, ks^{-1})	N_s	Variability Significance (σ)
1	$07^h23^m22\overset{s}{.}99$	$-27°26'10\overset{''}{.}1$	4.4	$2.8^{+0.9}_{-0.7}$	2.9	1.47
2	$07^h23^m22\overset{s}{.}34$	$-27°33'09\overset{''}{.}5$	4.4	$2.3^{+1.1}_{-0.7}$	3.9	1.09
3	$07^h23^m34\overset{s}{.}43$	$-27°23'32\overset{''}{.}4$	5.4	$2.4^{+1.1}_{-0.8}$	3.7	1.47
4	$07^h24^m34\overset{s}{.}95$	$-27°31'31\overset{''}{.}1$	6.1	$1.8^{+1.2}_{-0.7}$	5.5	1.01
5	$07^h23^m53\overset{s}{.}50$	$-27°23'06\overset{''}{.}5$	4.4	$0.6^{+0.3}_{-0.2}$	17	1.30
6	$07^h24^m27\overset{s}{.}89$	$-27°35'40\overset{''}{.}8$	6.5	$2.3^{+1.1}_{-0.7}$	3.9	2.48
7	$07^h23^m54\overset{s}{.}14$	$-27°42'29\overset{''}{.}5$	6.4	$2.2^{+1.0}_{-0.7}$	4.2	1.20
8	$07^h19^m30\overset{s}{.}22$	$-27°45'42\overset{''}{.}5$	4.1	$8.8^{+3.4}_{-2.4}$	0.5	0.44
9	$07^h19^m37\overset{s}{.}14$	$-27°33'12\overset{''}{.}0$	5.2	$2.4^{+1.1}_{-0.8}$	3.7	0.60
10	$07^h19^m25\overset{s}{.}72$	$-27°31'37\overset{''}{.}0$	5.8	$0.9^{+0.6}_{-0.3}$	12	0.36
11	$07^h19^m18\overset{s}{.}04$	$-27°25'15\overset{''}{.}4$	5.0	$1.7^{+0.9}_{-0.6}$	5.9	0.97
12	$07^h19^m41\overset{s}{.}92$	$-27°39'58\overset{''}{.}1$	5.0	$1.6^{+1.2}_{-0.7}$	6.4	1.02

convert the 0.3–10 keV XRT count-rates into 0.2–12 keV fluxes, using an absorbed power-law spectrum with a column of $N_H = 3 \times 10^{20}$ cm^{-2} and a power-law photon index $\Gamma = 1.7$, as used for 2XMM.[120] For each XRT source we then counted the number of 2XMMi-DR3 sources with values of the 0.2–12 keV flux—as measured with the EPIC MOS-1 camera (Turner et al. 2001) onboard *XMM-Newton*—at least as bright as the source in question. This was then scaled by the ratio of the *Swift*-XRT instantaneous FOV to the 2XMMi-DR3 unique sky coverage area (504 square degrees). This yielded, for each *Swift* source, the number of serendipitous sources (N_s) of at least that brightness expected in a single *Swift* FOV. These values, along with the count-rates, are given in Tables 3 and 4. For the January event we expected a total of 7.5 serendipitous sources, compared to our 8 detections; for the September event we expected 17 serendipitous sources, and had 12 detections. The number of serendipitous sources expected will not be a strong function of Galactic latitude at these latitudes ($-27\overset{\circ}{.}6$ for the January event and $-6\overset{\circ}{.}1$ for the September event) and flux levels; Galactic source sky densities are comparable to extragalactic values at a flux of around 5×10^{-14} erg cm^{-2} s^{-1} only at much lower latitudes, see, e.g., Motch et al. (2010).

In preparing for the event collection and *Swift* follow-up, we constructed a utility catalog that would allow us to look up the X-ray history of each field selected for observation in order to help determine if any of the observed sources coincide with known steady-state or variable sources. This X-ray source catalog, which we call XGWC,[121] combines public data from the HEASARC Master X-ray Catalog[122] and the GWGC. Upon examination of XGWC/HEASARC for known X-ray sources within the observed fields we found two X-ray sources (one of which was observed twice by *Swift*) in the catalog which were within the fields for the January event. Both were of unknown type. These catalog sources are likely to be associated with the reduced-threshold sources 3 and 4 reported in Table 3. The fields that were observed for the September event contained only one XGWC/HEASARC source of unknown type. This is likely to be associated with the reduced-threshold source 8 reported in Table 4.

We also performed a variability test on the observed sources, since an EM counterpart to the LIGO–Virgo event may be expected to be fading. To do this we produced a light curve of each source, creating one bin per *Swift* observation ID,[123] and

[120] http://xmmssc-www.star.le.ac.uk/Catalogue/2XMM/UserGuide_xmmcat.html#TabECFs

[121] http://aquarius.elte.hu/XGWC/index.html
[122] http://heasarc.gsfc.nasa.gov/W3Browse/all/xray.html
[123] For the September event we excluded the second observation of each source, since this was very short.

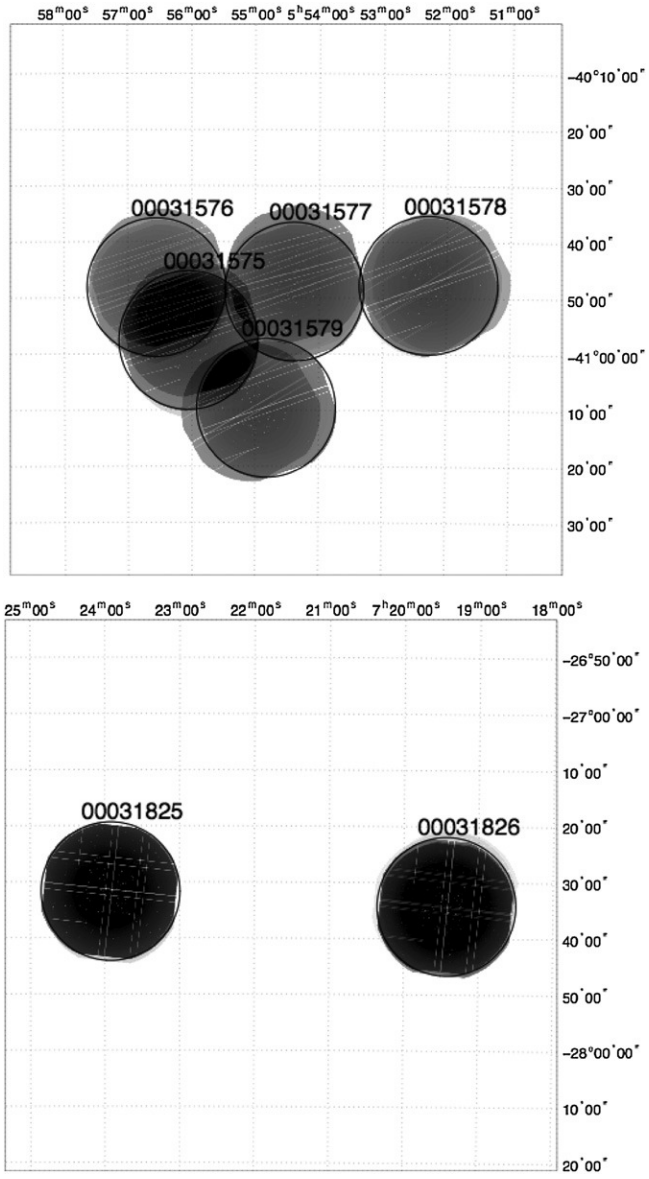

Figure 2. *Swift*-XRT image of the vicinity of the January event (top) and September event (bottom). The large circles show the fields of view of the various pointings. The gray scale denotes relative length of exposure at each location with darker colors indicating longer ones. The horizontal axis denotes right ascension (R.A.) in hours, minutes, and seconds and the vertical axis denotes declination (decl.) in degrees.

determining the count-rate using the Bayesian method (Kraft et al. 1991). The significance of any variability was then found simply by dividing the difference in the two bins by the errors in the two bins, added in quadrature. This is given in Tables 3 and 4; two sources show moderate (between 2σ and 2.5σ) evidence for variability (January source 1 and September source 6).

In addition to the observations reported above, a further follow-up observation was performed for the January trigger on 2010 January 30. This observation, ObsID 00031592001, contained 5.4 ks of data, centered at R.A. $= 88.^{\circ}73$, decl. $= -40.^{\circ}96$, i.e., overlapping heavily with field 00031577. Including the data from this field causes sources 1 and 4 to be registered as above-threshold detections. For source 4, the count-rate of the final observation was almost identical to the first; inclusion of this result changed the variability significance from 0.75σ to 0.04σ. For source 1, the addition of these data alters the variability only slightly, from 2.05σ to 1.98σ.

4.2. Optical and UV Results

The LIGO–Virgo target fields were observed by the *Swift* UVOT with the clear white filter (160–800 nm) or, if ground analysis indicated that the field contained a star too bright for observation in white, the broadband u filter (centered at 346.5 nm with full width at half-maximum of 78.5 nm) or narrow NUV $uvm2$ filter (centered at 224.6 nm with FWHM of 49.8 nm).

We first attempted to identify any UVOT counterparts to the X-ray reduced-threshold sources identified in the XRT images, photometering any source within $5''$ of the XRT position using the standard UVOTSOURCE code and calibrations from Poole et al. (2008) and Breeveld et al. (2011). The results are listed in Tables 5 and 6. For the January event, XRT reduced-threshold detection 7 fell off the smaller UVOT field and was not measured. UVOT counterpart sources to XRT reduced-threshold detections 1, 2, 3, and 4 were found in at least one epoch. However, they had corresponding sources in the Digital Sky Survey (DSS) and showed no photometric variation beyond the 1σ–2σ level. No counterparts to XRT reduced-threshold detections 5, 6, and 8 were found in UVOT.

For the September event, XRT reduced-threshold detections 1, 7, and 8 fell outside of the UVOT field. No counterparts to XRT reduced-threshold detections 2, 4, 11, and 12 were found by UVOT. Reduced-threshold detections 3 and 10 were also found by UVOT and correspond to DSS sources. XRT reduced-threshold detections 5, 6, and 9 correspond to very marginal detections in a crowded field and are either very faint objects or spurious detections. The apparent dimming of the UVOT counterpart to source 5 is spurious as this source was on the edge of one UVOT image and only a partial flux could be measured. In short, *no XRT reduced-threshold detection corresponds to either an optical transient or a variable source* for either the January or September event.

We next performed a blind search for variable targets within the field. In this instance, we photometered the entire field using the DAOPHOT (Stetson 1987) PSF photometry program. We photometered all data using a quadratically variable PSF and found photometry and image subtraction to be excellent, provided the PSF was based on stars not near the coincidence-loss limit of the data. Raw photometry was corrected for coincidence loss, exposure time, and large scale sensitivity. The number of detections in each field ranged from 250 to 2800 depending on the Galactic latitude of the field and the exposure time. Of the nearly 6800 sources that were detected in the UVOT data, approximately 5200 are well-measured point-like sources that are not near the coincidence-loss limit off the data. Of these, 11 are not near chip edges or bright stars but show very significant variability ($>7\sigma$) between the two epochs. Their coordinates are shown in Table 7. Such significant variability is likely to reflect real phenomena, such as active galaxies or variable stars, which are expected to be detected in any deep field. However, none of these variable sources corresponded to any X-ray detections and none show variability beyond a few 0.1 mag, which would be consistent with a tentative classification as normal variable stars or active galaxies. Further monitoring would be needed to determine their nature.

4.3. Summary of EM Findings

The XRT analysis produced 20 reduced-threshold detections and the UVOT analysis identified nearly 6800 sources in the follow-ups of the two events. However, all observations in

Table 5
UVOT Photometry for XRT Detections in the January Event

XRT Source No.	00031576001 White	00031577001 White	00031577002 White	00031578001 *u*	00031578002 *u*	00031592001 *uvm2*
1	...	...	...	...	...	19.83 ± 0.09
2	20.09 ± 0.06	...	...	...	...	...
3	...	17.70 ± 0.04	17.78 ± 0.04	...	...	...
4	...	19.50 ± 0.06	...	...	...	18.36 ± 0.04
5	...	...	...	>21.53	>21.33	...
6	...	...	...	>21.55	>21.27	...
7	...	...	...	...	...	...
8	...	...	...	>21.52	>21.40	...

Notes. Column headings designate UVOT fields and filters used and table entries are observed magnitudes. No XRT sources fell within the UVOT field of view for observations 00031575001, 00031575002, 00031576002, 00031579001, or 00031579002.

Table 6
UVOT Photometry for XRT Detections in the September Event

XRT Source No.	00031825001 *u*	00031825003 *u*	00031826001 White	00031826003 White
1	...	...	...	...
2	>20.73	>21.21	...	...
3	14.11 ± 0.02	14.11± 0.02	...	...
4	>20.76	>21.22	...	...
5	19.76 ± 0.17	20.67 ± 0.23	...	...
6	>20.79	21.10 ± 0.33	...	...
7	...	...	...	...
8	...	...	...	...
9	...	...	20.75 ± 0.36	20.32 ± 0.12
10	...	...	18.76 ± 0.07	18.90 ± 0.04
11	...	...	>20.79	...
12	...	...	>20.84	>21.65

Note. Column headings designate UVOT fields and filters used and table entries are observed magnitudes.

Table 7
Potential Variable Stars in UVOT Data

Variable Source No.	Right Ascension (R.A.) (J2000)	Declination (decl.) (J2000)	Filter	Mag	σ_M	Variability
V1	05:56:22.06	−40:58:38.3	White	19.77	0.018	8.03
V2	05:56:15.71	−40:56:06.8	White	20.51	0.026	9.73
V3	05:56:04.51	−40:51:50.3	White	20.50	0.020	7.14
V4	05:55:54.64	−40:59:55.3	White	19.29	0.017	6.35
V5	05:55:43.65	−40:55:51.9	White	21.04	0.029	6.88
V6	05:55:50.23	−40:45:40.8	White	19.38	0.063	12.10
V7	05:55:05.25	−41:04:07.9	White	16.53	0.008	14.93
V8	07:24:20.67	−27:33:36.5	*u*	17.26	0.013	9.67
V9	07:23:50.86	−27:30:24.8	*u*	17.82	0.024	8.74
V10	07:23:39.28	−27:25:38.5	*u*	19.42	0.030	7.29
V11	07:19:08.99	−27:37:35.0	White	16.27	0.044	14.50

X-ray, UV, and optical bands were consistent with expectations for serendipitous sources and no single source displayed significant variability in the XRT or UVOT analyses.

5. COMBINED GW–EM RESULTS

Information from the EM observations associated with a GW candidate event will have to be combined with GW data in order to establish key quantities associated with a combined GW–EM search for transients, like event significance or astrophysical reach. In this section we present a formalism for combining results from such joint observations. For the purpose of its validation we performed simulations using possible models of GW and EM signals. In the process we verified the overall search procedure and estimated the increase in sensitivity of the search which resulted from the *Swift* follow-up observations. Although this is presented within the context of the LIGO–Virgo–*Swift* search, it can be straightforwardly extended to other joint searches as well.

In the way the search was conducted, a typical joint candidate event is characterized by the strength of the GW signal expressed in terms of the coherent network amplitude η which is the detection statistic itself for coherent WaveBurst. This quantity is generally proportional to the signal-to-noise ratio and is described in detail in Klimenko et al. (2011) and in Abadie et al. (2012b). Joint candidate events are also characterized

by the measured X-ray flux, S, and the sky location of the X-ray source, $\Omega \equiv$ [R.A., decl.]. In addition to these, a skymap, i.e., the probability distribution for the location of a potential GW source, $p_{\rm m}(\Omega)$, is produced and used to select fields for imaging. We define the joint detection statistic for an event as the logarithm of the joint likelihood ratio, sometimes also referred to as the Bayes factor, given by

$$\Lambda_{\rm joint}(\eta, S, \Omega) = \Lambda_{\rm GW}(\eta)\Lambda_{\rm EM}(S)\Lambda_{\rm cor}(\Omega). \quad (2)$$

In the above equation $\Lambda_{\rm GW} = p(\eta\,|\,{\rm signal})/p(\eta\,|\,{\rm noise})$ is the likelihood ratio for a GW candidate, measuring its significance. $\Lambda_{\rm EM}(S) = p_0^{-1}(S)$ is the inverse of the probability density of observing an accidental, serendipitous X-ray source which is not correlated with the GW signal. The remaining term $\Lambda_{\rm cor}(\Omega) = p_{\rm m}(\Omega)$ is the probability for a GW source to be in the location of the X-ray source, which measures positional correlation between GW and EM signals. Detection statistics based on the likelihood ratio or the Bayes factor construction have been previously suggested and used in the context of searches for GW bursts (Clark et al. 2007; Cannon 2008; Abadie et al. 2011d) and GWs from compact binary coalescence (Abadie et al. 2010b; Biswas et al. 2012). In deriving Equation (2) (see the Appendix for details) we assumed that the dominant background in the EM sector is serendipitous X-ray sources that happen to be within the observed fields by chance. We neglected contributions to this from possible spurious sources—due to, e.g., instrumental artifacts—in the XRT analysis. In order to check if this assumption is justified we estimated from the 2XMMi-DR3 catalogue (Watson et al. 2009) that one expects to find at least one serendipitous source with flux equal or greater than 5.4×10^{-13} erg cm^{-2} s^{-1} within five *Swift* fields. Visual inspection of the XRT data would identify artifacts at or above this flux level, and they would be excluded from the analysis. No such artifacts were found in the fields analyzed in this paper. We also assumed that inhomogeneities in the distribution of serendipitous sources over the sky are small. As already mentioned, for every LIGO–Virgo candidate event *Swift* was nominally going to observe five $0.^{\circ}4 \times 0.^{\circ}4$ fields. The way the end-to-end search pipeline was constructed, only the most probable tiles according to the skymap $p_{\rm m}(\Omega)$ were observed as *Swift* fields. This resulted in a natural selection bias. As a result, the position correlation term, $\Lambda_{\rm cor}(\Omega)$, had a negligible effect in separation of real events from background events. After verifying this through simulations we drop it from the right-hand side of Equation (2), and the final expression for the detection statistic for the joint LIGO–Virgo and *Swift* search becomes

$$\rho_{\rm joint}(\eta, S) = \rho_{\rm GW}(\eta) + \rho_{\rm EM}(S), \quad (3)$$

where $\rho_{\rm GW}(\eta)$ and $\rho_{\rm EM}(S)$ are logarithms of $\Lambda_{\rm GW}(\eta)$ and $\Lambda_{\rm EM}(S)$, respectively.

We simulated the search by processing a population of model GW signals which were paired with plausible X-ray fluxes. The set of GW injections was the same with the one used previously (Abadie et al. 2012a) for methodological studies of joint GW–EM observations. These injections sampled the known galaxies within 50 Mpc according to the GWGC and were weighted to reflect each galaxy's blue light luminosity. Their intrinsic strength (at the source) spanned ad hoc standard candle values over three orders of magnitude. For the purpose of this analysis and to approximate a more realistic distribution of events that are relatively close to our detection threshold, we imposed that they fall below detectability, which implies $\eta \leqslant 3.5$, at distances outside the 50 Mpc range. For the low-latency search in 2009–2010, 3.5 was the typical threshold value for η. Translating this value into strain at the detector and ultimately at the source depends mildly on the waveform morphology and polarization state of the GW burst and rather strongly on the frequency content of it (Abadie et al. 2012b). In order to set the scale, at 50% detection efficiency during the 2009–2010 run and for GW bursts with energy content near 150Hz this value of η corresponds to an isotropic energy at the level of $5.6 \times 10^{-2}\, M_{\odot}c^2$ emitted in GWs from a hypothetical source at the Virgo Cluster (16 Mpc; Abadie et al. 2012b).

All such simulated events were added to LIGO and Virgo data and analyzed as in the actual search. We used these simulated GW signals to compute the coherent network amplitude, η, and its probability distribution, $p(\eta|{\rm signal})$, which is needed for calculation of the joint statistic in Equations (2) and (3). Models for X-ray counterparts were based on GRB afterglows observed by *Swift*. In order to set the scale of possible X-ray fluxes for counterparts, we considered several short hard GRBs and some bright and dim long GRBs (Zhang et al. 2009). The host galaxies of all selected GRBs had $z < 1$. We sampled the observed X-ray afterglow light curves for the observed GRBs at different time lags ($\sim 10^4$ s, 10^5 s, 10^6 s) relative to the time of arrival of the burst. For a possible X-ray counterpart to GWs from a source at 50 Mpc away this analysis gave us a wide range of flux values, $S_{50\,{\rm Mpc}}$, from 10^{-14} erg s^{-1} cm^{-2} to 10^{-8} erg s^{-1} cm^{-2}. In the absence of any other guidance, we performed simulations for each order of magnitude in that range. For a given $S_{50\,{\rm Mpc}}$ every GW signal was paired up with a corresponding X-ray flux, which was scaled up (as it was positioned anywhere within the 50 Mpc range) according to the distance to the source.

Computation of the joint detection statistic, Equation (3), also requires estimates of the background noise in GW detectors and flux distribution of serendipitous X-ray sources. Background noise in GW detectors is dominated by high amplitude instrumental artifacts. It is typically estimated by time-shifting data from one detector with respect to the other. In our simulations we used estimates for background noise from the coherent WaveBurst search for GW bursts with LIGO and Virgo in their 2010 science run (Abadie et al. 2012b). In the EM sector, on the other hand, serendipitous X-ray sources observed in coincidence with a GW signal are the main source of false alarms. As in assessing the background in the XRT analysis we presented in Section 4.1, we used also here the 2XMMi-DR3 catalogue (Watson et al. 2009) of serendipitous sources for the estimation of the flux distribution for such sources. For both types of backgrounds we fitted analytical models to the data and computed $p(\eta|{\rm noise})$ and $p_0^{-1}(S)$ appearing in the definition of the joint likelihood ratio in Equation (2).

For each simulated GW signal complemented by an X-ray counterpart of a given flux, the last step of the analysis involved the calculation of the joint detection statistic $\rho_{\rm joint}$ as given by Equation (3). Using estimates for the GW and X-ray backgrounds, the false alarm probability (FAP) of observing a background event with joint statistic $\rho'_{\rm joint} \geqslant \rho_{\rm joint}$ in a month long search was computed. This defined the significance of the observed event. Figure 3 shows the efficiency in detecting these simulated GW–EM signals as a function of FAP, P_0, in a joint LIGO–Virgo-*Swift* search using five or ten *Swift* fields and for a wide range of X-ray counterpart fluxes. The efficiency is defined as the fraction of simulated signals with FAP, $P'_0 \leqslant P_0$. For comparison, we also plot the efficiency curve for the GW only search which does not use any (*Swift*) EM follow-up.

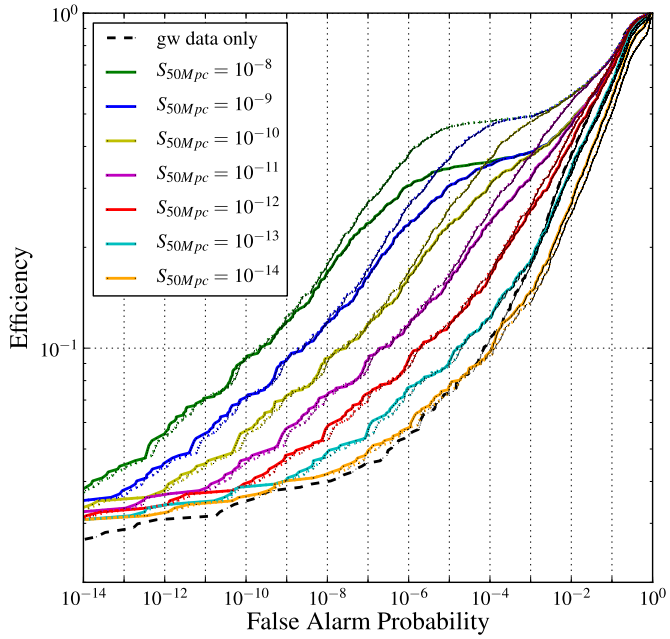

Figure 3. Efficiency as a function of false alarm probability for the joint LIGO–Virgo and *Swift* search. The solid (dotted) curves represent performance of the joint search with five (ten) fields observed by *Swift* for various values of the flux of an X-ray counterpart (in units of erg s^{-1} cm^{-2}) at a distance of 50 Mpc, $S_{50\,\mathrm{Mpc}}$. The dashed line is the curve for the GW only search.

In the rare-event region below FAP of 10^{-4} (i.e., corresponding to below $\sim 4\sigma$ for the case of Gaussian statistics) one can see how at fixed event significance the efficiency can improve by a significant factor depending on the associated EM flux that is measured. As expected, the gain increases with the brightness of the X-ray counterpart. It reaches a saturation point at which roughly one-third and one-half, respectively, of the signals are detected in the searches with five and ten fields observed by *Swift*. This is determined by the number of signals for which their true location overlapped with the five (or ten) most significant tiles of the skymap. Only these signals were observed by *Swift*. The rest of the signals were "missed" in the follow-up and therefore did not benefit from it. Observing more fields with *Swift* increases the chances of locating the X-ray counterpart, but at the same time has the negative effect of increasing chances of accidental detection of serendipitous X-ray sources (background). Figure 3 shows that the net gain is noteworthy if ten instead of five fields were observed by *Swift*. In general, an XRT with a wide FOV would be optimal for the purpose of the joint search. We should note though that for such a telescope the position correlation term, $\Lambda_{\mathrm{cor}}(\Omega)$, in the joint likelihood ratio Equation (2) may become important and should be included in the analysis.

6. SUMMARY AND DISCUSSION

During two periods in late 2009 and 2010 the LIGO–Virgo GW interferometric network sent out low-latency candidate GW events to partner observatories for rapid follow-ups in various EM bands. Two such events were followed up as ToOs by *Swift*. One of the events followed up by *Swift* was ultimately revealed to be a blind injection artificially inserted into the data as a test of the system (Abadie et al. 2011c) and the other was a reduced-threshold test event (Abadie et al. 2011b, 2012b). Prompt analysis of both the XRT and UVOT data obtained from the seven total fields observed showed results consistent with expectations for serendipitous sources. Given the lack of EM candidates standing out above background, these particular observations do not increase our confidence in the validity of the GW transients as established by the GW detectors alone.

Combining GW and EM astronomy will be pivotal in maximizing the science in the advanced detector era of gravitational interferometers; it may not only increase our confidence in the detection of GWs but also complete our understanding of the astrophysics of the observed systems (Bloom et al. 2009; Phinney 2009; Stamatikos et al. 2009; Metzger & Berger 2012). Our prototype observing program and end-to-end analysis has been the first step in joint X-ray and GW observations. We demonstrated their feasibility and the considerable added value joint observations bring. Improvements to these will continue to be made in the future on both the EM and GW side. The relatively narrow FOV of instruments such as *Swift* with respect to the limited pointing resolution abilities of GW interferometers makes identifying the position of the source on the sky non-trivial. A possible fourth detector site in India, Japan, or elsewhere and continued refinements in source localization algorithms are likely to reduce the sky-position error area. On the EM side, a more highly optimized faint source detection scheme for XRT transients might yield improvement in EM sensitivity. In late 2011 *Swift* implemented onboard software changes to allow automatic scheduling sequences of partially overlapping XRT FOV exposures in response to ToO observation requests for targets with position uncertainties larger than the FOV—this will assist the follow-up of GW targets. A significant role will also be played by prompt follow-up campaigns in the optical band that may provide rapid sub-degree source localizations. Such localizations may facilitate the subsequent follow-up with narrow FOV instruments including *Swift*, thus significantly improving the chances of capturing the X-ray signatures of GW sources.

In order to carry out multimessenger astrophysics with GWs, it will be extremely important to have *Swift* and/or *Swift*-like satellites capable of rapid pointing, multi-wavelength observations and of as wide an FOV as possible operating concurrently with the advanced GW detector network later in this decade. Maximizing the science from GW astronomy will require sensitive partner instruments all across the EM spectrum. The successful completion of this end-to-end program of EM follow-ups by *Swift* and other observatories during the most recent science runs of the LIGO–Virgo network provides confidence that such joint observations will be both technically feasible and scientifically valuable endeavors in the future.

The authors gratefully acknowledge the support of the United States National Science Foundation for the construction and operation of the LIGO Laboratory, the Science and Technology Facilities Council of the United Kingdom, the Max-Planck-Society, and the State of Niedersachsen/Germany for support of the construction and operation of the GEO600 detector, and the Italian Istituto Nazionale di Fisica Nucleare and the French Centre National de la Recherche Scientifique for the construction and operation of the Virgo detector. The authors also gratefully acknowledge the support of the research by these agencies and by the Australian Research Council, the International Science Linkages program of the Commonwealth of Australia, the Council of Scientific and Industrial Research of India, the Istituto Nazionale di Fisica Nucleare of Italy, the Spanish Ministerio de Economía y Competitividad, the Conselleria d'Economia Hisenda i Innovació of the Govern de les Illes Balears, the

Foundation for Fundamental Research on Matter supported by the Netherlands Organisation for Scientific Research, the Polish Ministry of Science and Higher Education, the FOCUS Programme of Foundation for Polish Science, the Royal Society, the Scottish Funding Council, the Scottish Universities Physics Alliance, The National Aeronautics and Space Administration, the Carnegie Trust, the Leverhulme Trust, the David and Lucile Packard Foundation, the Research Corporation, and the Alfred P. Sloan Foundation. This work was also partially supported through a NASA grant/cooperative agreement number NNX09AL61G to the Massachusetts Institute of Technology. P. Evans and J. P. Osborne acknowledge financial support from the UK Space Agency.

APPENDIX

DERIVATION OF THE JOINT LIKELIHOOD RATIO

In this section we derive from first principles equation (2) that we used in Section 5 in order to establish the detection statistic of the joint GW–EM search. Using Bayes' theorem, the probability skymap for a potential GW source, $p_{\rm m}(\Omega)$, can be written as

$$p_{\rm m}(\Omega \,|\, \eta, \text{signal}) = \frac{p(\eta \,|\, \Omega, \text{signal}) p(\Omega \,|\, \text{signal})}{p(\eta \,|\, \text{signal})}, \quad \text{(A1)}$$

where $p(\eta \,|\, \Omega, \text{signal})$ and $p(\eta \,|\, \text{signal})$ are the conditional probabilities to measure a GW signal with coherent network amplitude η in the case of a source located at Ω and a source with unknown location, respectively; $p(\Omega \,|\, \text{signal})$ is the prior probability distribution for source location, which in this search is determined by the distribution of galaxies in the GWGC catalog and distance weighting, see Equation (1).
The joint likelihood ratio is defined as

$$\Lambda_{\rm joint}(\eta, S, \Omega) = \frac{p(\eta, S, \Omega \,|\, \text{signal})}{p(\eta, S, \Omega \,|\, \text{noise})} = \frac{\int p(\eta \,|\, \Omega', \text{signal}) p(S, \Omega \,|\, S', \Omega', \text{signal}) p(\Omega' \,|\, \text{signal}) p(S' \,|\, \text{signal}) \, d\Omega' \, dS'}{p(\eta \,|\, \text{noise}) p_0(S)}, \quad \text{(A2)}$$

where $p_0(S)$ is the probability density of observing an accidental, serendipitous X-ray source that is not correlated with the GW signal, and we introduce $p(S, \Omega \,|\, S', \Omega', \text{signal})$, the probability distribution of flux, S, and X-ray source location, Ω, as measured by *Swift* for a source whose true flux at the detector and location are S' and Ω', respectively; $p(S' \,|\, \text{signal})$ is the prior probability distribution for the flux of an X-ray counterpart to the GW signal. Integration in the numerator is performed over all possible values of flux and sky locations. Note that, although we assume the strength of the GW signal to be uncorrelated with the flux of the X-ray counterpart, we demand that both types of signals originate from the same sky position, Ω'. This enforces correlation between measured locations of GW and its X-ray counterpart.

Using Equation (A1) we can express the joint likelihood ratio in terms of the skymap, $p_{\rm m}(\Omega)$, and GW likelihood ratio, $\Lambda_{\rm GW}(\eta) = p(\eta \,|\, \text{signal}) / p(\eta \,|\, \text{noise})$:

$$\Lambda_{\rm joint}(\eta, S, \Omega) = \Lambda_{\rm GW}(\eta) \times \frac{\int p_{\rm m}(\Omega') p(S, \Omega \,|\, S', \Omega', \text{signal}) p(S' \,|\, \text{signal}) \, d\Omega' \, dS'}{p_0(S)}. \quad \text{(A3)}$$

This expression can be simplified further by postulating $p(S, \Omega \,|\, S', \Omega', \text{signal}) = \delta(S - S')\delta(\Omega - \Omega')$ and $p(S' \,|\, \text{signal}) = 1$,

$$\Lambda_{\rm joint}(\eta, S, \Omega) = \Lambda_{\rm GW}(\eta) \frac{p_{\rm m}(\Omega)}{p_0(S)}. \quad \text{(A4)}$$

Defining $\Lambda_{\rm EM}(S) = p_0^{-1}(S)$ and $\Lambda_{\rm cor}(\Omega) = p_{\rm m}(\Omega)$, we arrive at the form for the joint likelihood ratio given in Equation (2). We stress that the particular form of $\Lambda_{\rm EM}(S)$ and $\Lambda_{\rm cor}(\Omega)$ is a consequence of the simplifying assumptions about *Swift*'s ability to measure the flux and location of an X-ray source that are justified in Section 5. In general, these quantities are going to be non-trivial ratios of likelihoods estimating odds of an X-ray candidate source to be a counterpart to GW based on its brightness and location.

REFERENCES

Abadie, J., Abbott, B. P., Abbott, R., et al. 2010a, Class. Quant. Grav., 27, 173001
Abadie, J., Abbott, B. P., Abbott, R., et al. 2010b, Phys. Rev. D, 82, 102001
Abadie, J., Abbott, B. P., Abbott, R., et al. 2011a, A&A, 541, A155
Abadie, J., Abbott, B. P., Abbott, R., et al. 2011b, Phys. Rev. D, 85, 082002
Abadie, J., Abbott, B. P., Abbott, R., et al. 2011c, http://www.ligo.org/news/blind-injection.php
Abadie, J., Abbott, B. P., Abbott, R., et al. 2011d, Phys. Rev. D, 83, 042001
Abadie, J., Abbott, B. P., Abbott, R., et al. 2012a, A&A, 539, A124
Abadie, J., Abbott, B. P., Abbott, R., et al. 2012b, Phys. Rev. D, 85, 122007
Abbott, B. P., Abbott, R., Adhikari, R., et al. 2009, Rep. Prog. Phys., 72, 076901
Accadia, T., Acernese, F., Alshourbagy, M., et al. 2012, J. Instrum., 7, P03012
Anders, E., & Grevesse, N. 1989, Geochim. Cosmochim. Acta, 53, 197
Barthelmy, S. D., Barbier, L. M., Cummings, J. R., et al. 2005, Space Sci. Rev., 120, 143
Berger, E. 2009, ApJ, 690, 231
Berger, E. 2011, New Astron. Rev., 55, 1
Berger, E., Price, P. A., Cenko, S. B., et al. 2005, Nature, 438, 988
Biswas, R., Brady, P. R., Burguet-Castell, J., et al. 2012, Phys. Rev. D, 85, 122008
Bloom, J. S., Holz, D. E., Hughes, S. A., et al. 2009, arXiv:0902.1527
Bloom, J. S., Kulkarni, S. R., Djorgovski, S. G., et al. 1999, Nature, 401, 453
Breeveld, A. A., Landsman, W., Holland, S. T., et al. 2011, in AIP Conf. Proc. 1358, Gamma Ray Bursts 2010, ed. J. E. McEnery, J. L. Racusin, & N. Gehrels (Melville, NY: AIP), 373
Burrows, D. N., Hill, J. E., Nousek, J. A., et al. 2005, Space Sci. Rev., 120, 165
Cannon, K. 2008, Class. Quantum Grav., 25, 105024
Clark, J., Heng, I. S., Pitkin, M., & Woan, G. 2007, Phys. Rev. D, 76, 043003
Corsi, A., & Mészáros, P. 2009, ApJ, 702, 1171
Evans, P. A., Beardmore, A. P., Page, K. L., et al. 2007, A&A, 469, 379
Evans, P. A., Beardmore, A. P., Page, K. L., et al. 2009, MNRAS, 397, 1177
Fryer, C. L., Holz, D. E., & Hughes, S. A. 2002, ApJ, 565, 430
Gehrels, N., Chincarini, G., Giommi, P., et al. 2004, ApJ, 611, 1005
Gehrels, N., Sarazin, C. L., O'Brien, P. T., et al. 2005, Nature, 437, 851
Goad, M. R., Tyler, L. G., Beardmore, A. P., et al. 2007, A&A, 476, 1401
Jansen, F., Lumb, D., Altieri, B., et al. 2001, A&A, 365, L1
Kalberla, P. M. W., Burton, W. B., Hartmann, D., et al. 2005, A&A, 440, 775
Klimenko, S., Vedovato, G., Drago, M., et al. 2011, Phys. Rev. D, 83, 102001
Kochanek, C. S., & Piran, T. 1993, ApJ, 417, L17
Kopparapu, R., Hanna, C., Kalogera, V., et al. 2008, ApJ, 675, 1459
Kraft, R. P., Burrows, D. N., Nousek, J. A., et al. 1991, ApJ, 374, 344
Kulkarni, S. R., Frail, D. A., Wieringa, M. H., et al. 1998, Nature, 395, 663
Matheson, T., Garnavich, P. M., Stanek, K. Z., et al. 2003, ApJ, 599, 394
Mészáros, P. 2006, Rep. Prog. Phys., 69, 2259
Metzger, B. D., & Berger, E. 2012, ApJ, 746, 48
Metzger, B. D., Martinez-Pinedo, G., Darbha, S., et al. 2010, MNRAS, 406, 2650
Motch, C., Warwick, R., Cropper, M. S., et al. 2010, A&A, 523, A92
Nakar, E. 2007, Phys. Rep., 442, 166
Nuttall, L., & Sutton, P. J. 2010, Phys. Rev. D, 82, 102002
Phinney, E. S. 1991, ApJ, 380, L17
Phinney, E. S. 2009, Astro2010: The Astronomy and Astrophysics Decadal Survey, Science White Papers, 235
Piran, T. 2004, Rev. Mod. Phys., 76, 1143

Poole, T. S., Breeveld, A. A., Page, M. J., et al. 2008, MNRAS, 383, 627
Roming, P. W. A., Kennedy, T. E., Mason, K. O., et al. 2005, Space Sci. Rev., 120, 95
Schutz, B. F. 1986, Nature, 323, 310
Soderberg, A. M., Brunthaler, A., Nakar, E., et al. 2010, ApJ, 725, 922
Soderberg, A. M., Kulkarni, S. R, Fox, D. B., et al. 2005, ApJ, 627, 877
Stamatikos, M., Gehrels, G., Halzen, F., et al. 2009, Astro2010: The Astronomy and Astrophysics Decadal Survey, Science White Papers, 284
Stetson, P. B. 1987, PASP, 99, 191
Stubbs, C. W. 2008, Class. Quantum Grav., 25, 184033
Sylvestre, J. 2003, ApJ, 591, 1152
Turner, M. J. L., Abbey, A., Arnaud, M., et al. 2001, A&A, 365, L27
Watson, M. G., Schröder, A. C., Fyfe, D., et al. 2009, A&A, 493, 339
White, D. J., Daw, E. J., & Dhillon, V. S. 2011, Class. Quant. Grav., 28, 085016
Zhang, B., Zhang, B.-B., Virgili, F. J., et al. 2009, ApJ, 703, 1696
Zhang, W., & MacFadyen, A. 2009, ApJ, 698, 1261